THE JOURNAL OF BIOLOGICAL CHEMISTRY VOL. 292, NO. 1, pp. 146–160, January 6, 2017

Sortilin 1 Modulates Hepatic Cholesterol Lipotoxicity in Mice via Functional Interaction with Liver Carboxylesterase 1*

Received for publication, October 4, 2016, and in revised form, November 19, 2016 Published, JBC Papers in Press, November 23, 2016, DOI 10.1074/jbc.M116.762005

Jibiao Li‡, Yifeng Wang‡, David J. Matye‡, Hemantkumar Chavan‡, Partha Krishnamurthy‡, Feng Li§, and Tiangang Li‡1

From the ‡Department of Pharmacology, Toxicology and Therapeutics, Kansas University Medical Center, Kansas City, Kansas 66160 and the §Department of Molecular and Cellular Biology, Baylor College of Medicine, Houston, Texas 77030

Edited by George M. Carman

The liver plays a key role in cholesterol metabolism. Impaired hepatic cholesterol homeostasis causes intracellular free cholesterol accumulation and hepatocyte injury. Sortilin 1 (SORT1) is a lysosomal trafficking receptor that was identified by genome-wide association studies (GWAS) as a novel regulator of cholesterol metabolism in humans. Here we report that SORT1 deficiency protected against cholesterol accumulation-induced liver injury and inflammation in mice. Using an LC-MS/MS-based proteomics approach, we identified liver carboxylesterase 1 (CES1) as a novel SORT1-interacting protein. Mechanistic studies further showed that SORT1 may regulate CES1 lysosomal targeting and degradation and that SORT1 deficiency resulted in higher liver CES1 protein abundance. Previous studies have established an important role of hepatic CES1 in promoting intracellular cholesterol mobilization, cholesterol efflux, and bile acid synthesis. Consistently, high cholesterol atherogenic diet-challenged *Sort1* knock-out mice showed less hepatic free cholesterol accumulation, increased bile acid synthesis, decreased biliary cholesterol secretion, and the absence of gallstone formation. SORT1 deficiency did not alter hepatic ceramide and fatty acid metabolism in high cholesterol atherogenic diet-fed mice. Finally, knockdown of liver CES1 in mice markedly increased the susceptibility to high cholesterol diet-induced liver injury and abolished the protective effect against cholesterol lipotoxicity in *Sort1* knock-out mice. In summary, this study identified a novel SORT1-CES1 axis that regulates cholesterol-induced liver injury, which provides novel insights that improve our current understanding of the molecular links between SORT1 and cholesterol metabolism. This study further suggests that therapeutic inhibition of SORT1 may be beneficial in improving hepatic cholesterol homeostasis in metabolic and inflammatory liver diseases.

Sortilin 1 (SORT1) is a trans-membrane multi-ligand receptor that mainly localizes in the trans-Golgi network (TGN)[2] (1). A major function of SORT1 is to deliver various protein ligands in trafficking vesicles to the late endocytic compartments. Some of these proteins are lysosome-resident enzymes, and others are targeted for lysosome degradation (2, 3). A number of genome-wide association studies (GWAS) revealed that *SORT1* gene was strongly associated with plasma low density lipoprotein cholesterol levels in large human populations (4, 5), supporting an important role of SORT1 in cholesterol metabolism in humans. A number of studies have suggested that hepatic SORT1 may modulate hepatic lipoprotein production and plasma lipoprotein clearance (3, 6–10), but findings from these studies are somewhat controversial. The role and mechanisms of SORT1 regulation of cholesterol metabolism in various forms of metabolic and inflammatory diseases are incompletely understood, and further studies are required.

Hepatic cholesterol accumulation causes mitochondrial dysfunction, lysosome impairment, and hepatic injury, and has been implicated in the pathogenesis of liver diseases including non-alcoholic steatohepatitis (11–19). Here we report that mice deficient in SORT1 were protected against cholesterol-induced liver injury. Using an unbiased LC-MS/MS-based proteomics approach, we identified a novel SORT1-interacting protein called human liver carboxylesterase 1 (CES1, also known as cholesteryl ester hydrolase in humans) in HepG2 cells and mouse CES1 (also known as esterase-X (Es-X)) in mouse liver. CES1 is a neutral hydrolase for cholesterol ester and triglyceride and plays an important role in hepatic lipid mobilization (20–22). A number of previous studies have shown that CES1 prevents lipid accumulation in the liver (22–24) and in macrophages (21, 25). Of particular interest is that hepatocyte CES1 has been shown to promote cholesterol entering into the bile acid synthetic pathways for sterol elimination (20, 26). Here we showed that SORT1 may control CES1 abundance by mediating CES1 lysosomal targeting and degradation, and higher liver CES1 levels and increased bile acid synthesis may mediate

* This work was supported in part by an American Diabetes Association Junior Faculty Award (to T. L.), National Institutes of Health Grant 1R01DK102487-01 (to T. L.), National Center for Research Resources Grant 5P20RR021940-07, and NIGMS Grants 8 P20 GM103549-07 and P30GM118247 from the National Institutes of Health. The authors declare that they have no conflicts of interest with the contents of this article. The content is solely the responsibility of the authors and does not necessarily represent the official views of the National Institutes of Health.

[1] To whom correspondence should be addressed: Dept. of Pharmacology, Toxicology and Therapeutics, The University of Kansas Medical Center, 3901 Rainbow Blvd., Kansas City, KS 66160. Tel.: 913-588-9974; Fax: 913-588-7501; E-mail: tli@kumc.edu.

[2] The abbreviations used are: TGN, trans-Golgi network; FC, free cholesterol; CE, cholesterol ester; HCD, high cholesterol diet; AST, aspartate transaminase; ALT, alanine transaminase; ACAT, acyl-CoA:cholesterol acyltransferase; LDLR, low density lipoprotein receptor; AA, amino acid; CQ, chloroquine; CA, cholic acid; CDCA, chenodeoxycholic acid; MCA, muricholic acid; UDCA, ursodeoxycholic acid; SHP, small heterodimer partner; FXR, farnesoid X receptor; IP, immunoprecipitation; Es-X, esterase-X; Ad, adenovirus; STED, stimulated emission depletion; MOI, multiplicity of infection.

the protection against cholesterol lipotoxicity in *Sort1* knockout (*Sort1* KO) mice. This study provides novel mechanistic insights linking liver SORT1 function to cholesterol metabolism and suggests that therapeutic inhibition of hepatic SORT1 may be beneficial in improving hepatic cholesterol homeostasis in liver diseases.

Results

SORT1-deficient Mice Show Attenuated Cholesterol-induced Liver Injury—We first challenged WT and *Sort1* KO mice with a high cholesterol/cholate atherogenic diet (HCD), which has been shown to induce robust hepatic cholesterol accumulation, oxidative stress, mitochondrial impairment, and liver injury (13, 14). WT and *Sort1* KO mice showed similar body weight after 1 week and 6 weeks of HCD feeding (not shown), but liver to body weight ratio was significantly lower in 6-week HCD-fed *Sort1* KO mice (Fig. 1*A*). Livers of HCD-fed WT mice gradually showed swollen hepatocytes with pale vacuolated cytoplasm (Fig. 1*B*), consistent with histological characteristics of hepatocyte injury and hydropic degeneration (14, 27). These histological features were attenuated in *Sort1* KO mice at both 1-week and 6-week time points (Fig. 1*B*). Furthermore, hepatic inflammatory infiltration, as evidenced by both H&E and F4/80 macrophage marker staining, was significantly less in 6-week HCD-fed *Sort1* KO mice (Fig. 1, *B* and *C*). Consistently, 6-week HCD-fed *Sort1* KO mice showed lower plasma AST and ALT levels than WT controls, suggesting attenuated liver injury (Fig. 1*D*). Liver monocyte chemoattractant protein 1 (MCP1) mRNA was gradually induced by HCD feeding in WT mice (Fig. 1*E*). Liver MCP1 mRNA was significantly lower in 1-week HCD-fed *Sort1* KO mice, and trended lower in 6-week HCD-fed *Sort1* KO mice when compared with WT controls (Fig. 1*E*). mRNA levels of hepatic cytokines TNFα and IL-1β were not induced after 1 week of HCD feeding, but were significantly induced after 6 weeks of HCD feeding in the WT group. After 6 weeks of HCD feeding, *Sort1* KO mice showed significantly lower IL-1β mRNA, but not TNFα mRNA, when compared with WT controls (Fig. 1*E*). These results generally indicate attenuated HCD-induced liver injury in *Sort1* KO mice.

HCD-fed Sort1 KO Mice Had Reduced Hepatic Free Cholesterol Accumulation—HCD feeding to WT mice caused rapid hepatic cholesterol ester (CE) and free cholesterol (FC) elevation at 1 week (Fig. 2*A*). At 6 weeks, hepatic FC levels continued to increase without further increase of hepatic CE levels. Because the hepatocytes respond to higher cholesterol influx by converting excessive cholesterol mainly to CE to be stored in the lipid droplets, it is possible that this ability was exceeded at 6 weeks of HCD feeding, and the liver started to accumulate more FC without further CE increase (Fig. 2, *A* and *B*). HCD-fed *Sort1* KO mice accumulated significantly less FC in the liver when compared with WT mice (Fig. 2*A*), which is in line with attenuated liver injury in these mice. Elevated intracellular FC was shown to damage mitochondrial function as a key cause of hepatocyte injury (13). Consistently, freshly isolated liver mitochondria from HCD-fed *Sort1* KO mice showed significantly improved respiratory function when compared with WT (Fig. 2*B*). In addition, we found that plasma AST levels, as a marker of liver injury, were strongly associated with hepatic FC levels among 6-week HCD-fed WT and *Sort1* KO mice ($r = 0.91$) (Fig. 2*C*). To further determine the relationship between cellular cholesterol accumulation and cell injury, we next performed cholesterol loading in cultured HepG2 cells as an *in vitro* model. We showed that a modest elevation of cellular cholesterol induced by cholesterol loading was sufficient to cause cell injury as evidenced by an increased number of TUNEL-positive cells and modestly higher caspase-3 activity (Fig. 2, *D–F*). Furthermore, treating cells with an acyl-CoA:cholesterol acyltransferase (ACAT) inhibitor to block FC esterification to CE resulted in decreased cellular CE and increased cellular FC (Fig. 2*D*). Although this further cellular FC elevation caused by ACAT inhibition was very modest (~15%), it led to a significantly increased number of TUNEL-positive cells and further elevated caspase-3 activity (Fig. 2, *E* and *F*). These *in vivo* and *in vitro* results collectively suggest that cellular FC accumulation caused hepatocyte injury, and attenuated liver injury in HCD-fed *Sort1* KO mice was at least partly due to lower hepatic FC accumulation.

Attenuated Liver Injury in Sort1 KO Mice Was Not due to Altered Ceramide Signaling—Cellular cholesterol and fatty acids can affect ceramide metabolism and signaling, which in turn mediates lipotoxic cell injury (28–30). The acid sphingomyelinase, which hydrolyzes sphingomyelins to ceramides in the lysosome, was shown to be involved in cytokine-induced hepatocyte death and diet-induced steatohepatitis (31). SORT1 has been implicated in the regulation of acid sphingomyelinase trafficking to the lysosomes (32). A recent study suggested that SORT1 deficiency decreased acid sphingomyelinase activity and thus may affect ceramide production in diet-induced obesity (33). We directly measured the levels of sphingolipid and fatty acid species in mouse livers. However, no differences in hepatic sphingomyelin species or C16:0 ceramide, which is the major ceramide species involved in liver injury (30), were observed between WT and *Sort1* KO mice on HCD diet (Fig. 3*A*). In addition, hepatic triglyceride, free fatty acid species, and ketone body β-hydroxybutyrate, a marker for fatty acid oxidation, were not significantly different between WT and *Sort1* KO mice (Fig. 3, *B–D*). These results ruled out the possible involvement of ceramide signaling in attenuated liver injury in HCD-fed *Sort1* KO mice.

HCD-fed Sort1 KO Mice Showed Decreased Biliary Cholesterol Secretion and Were Protected against Gallstone Formation—Biliary cholesterol secretion is a major pathway for liver FC elimination, and was thus investigated next. We first noticed that HCD feeding for 6 weeks, but not 1 week (not shown), induced cholesterol gallstone formation in all WT mice (Fig. 4*A*). In contrast, no gallstones were presented in *Sort1* KO mice. Biochemical measurements determined that HCD-fed *Sort1* KO mice had ~50% less gallbladder cholesterol than WT mice (Fig. 4*B*). Both gallbladder phospholipid and bile acids tended to be higher in HCD-fed *Sort1* KO mice, but these increases did not reach statistical significance (Fig. 4*B*). Correlation analysis further found that gallbladder total cholesterol levels strongly and positively correlated with hepatic total cholesterol levels among HCD-fed WT and *Sort1* KO mice (Fig. 4*C*). We therefore challenged mice with HCD for 1 week and measured biliary lipid secretion rate. Consistently, *Sort1* KO

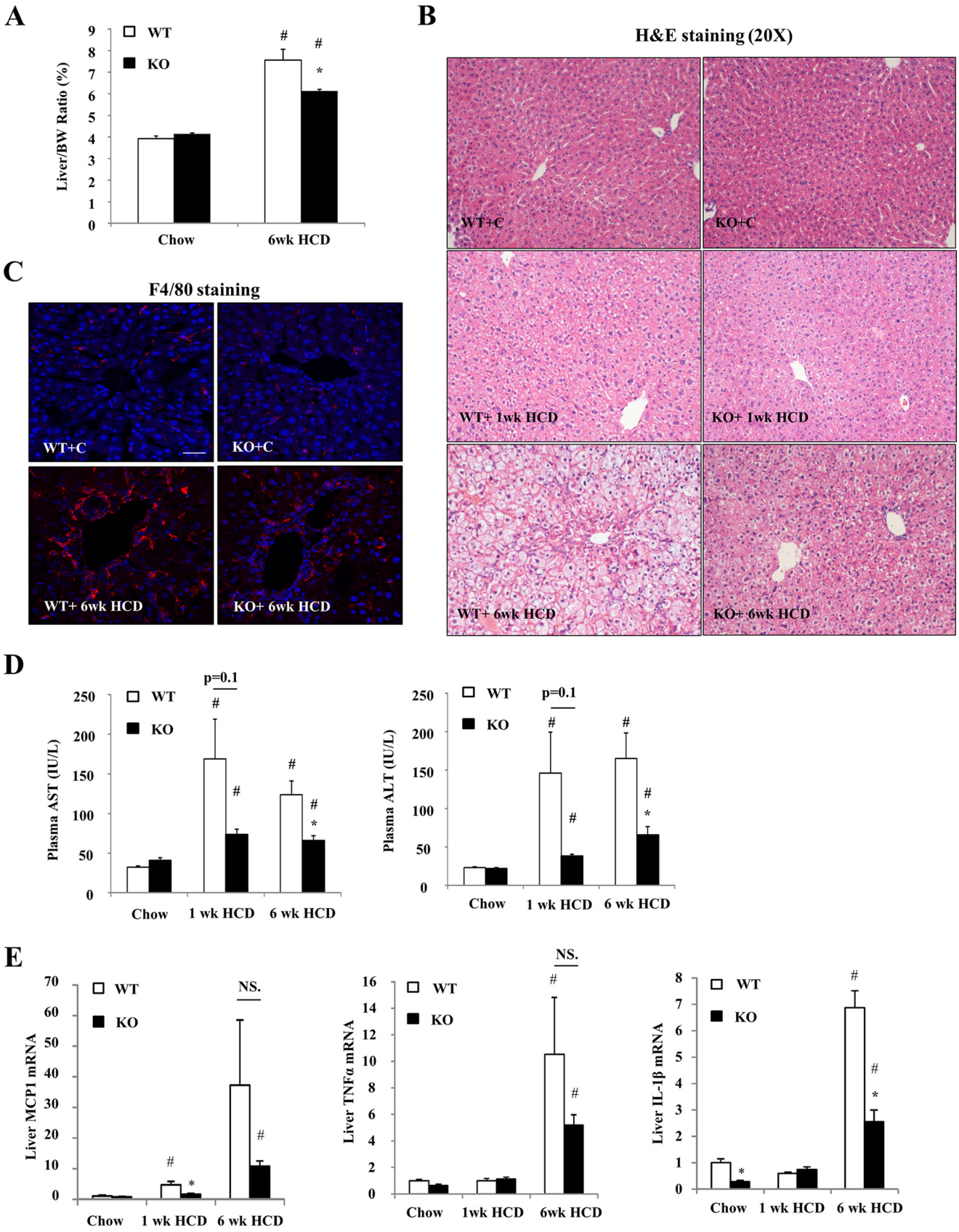

FIGURE 1. ***Sort1* KO mice were protected against HCD-induced liver injury.** WT and *Sort1* KO mice were fed a chow diet or an HCD for 1 week or 6 weeks. Mice were fasted overnight (~16 h) before sacrifice. *A*, liver to body weight (*BW*) ratio. *B*, H&E staining of liver sections. *WT+C*, WT plus chow diet; *KO+C*, knock-out plus chow diet. *C*, F4/80 immunostaining of liver sections. *Scale bar*: 50 μm. *D*, plasma AST and ALT. *E*, liver mRNA expression. All results are expressed as mean ± S.E. $n = 4–6$. * indicates statistical significance, *versus* WT mice on same diet. # indicates statistical significance, *versus* chow-fed mice of the same genotype. NS, not significant.

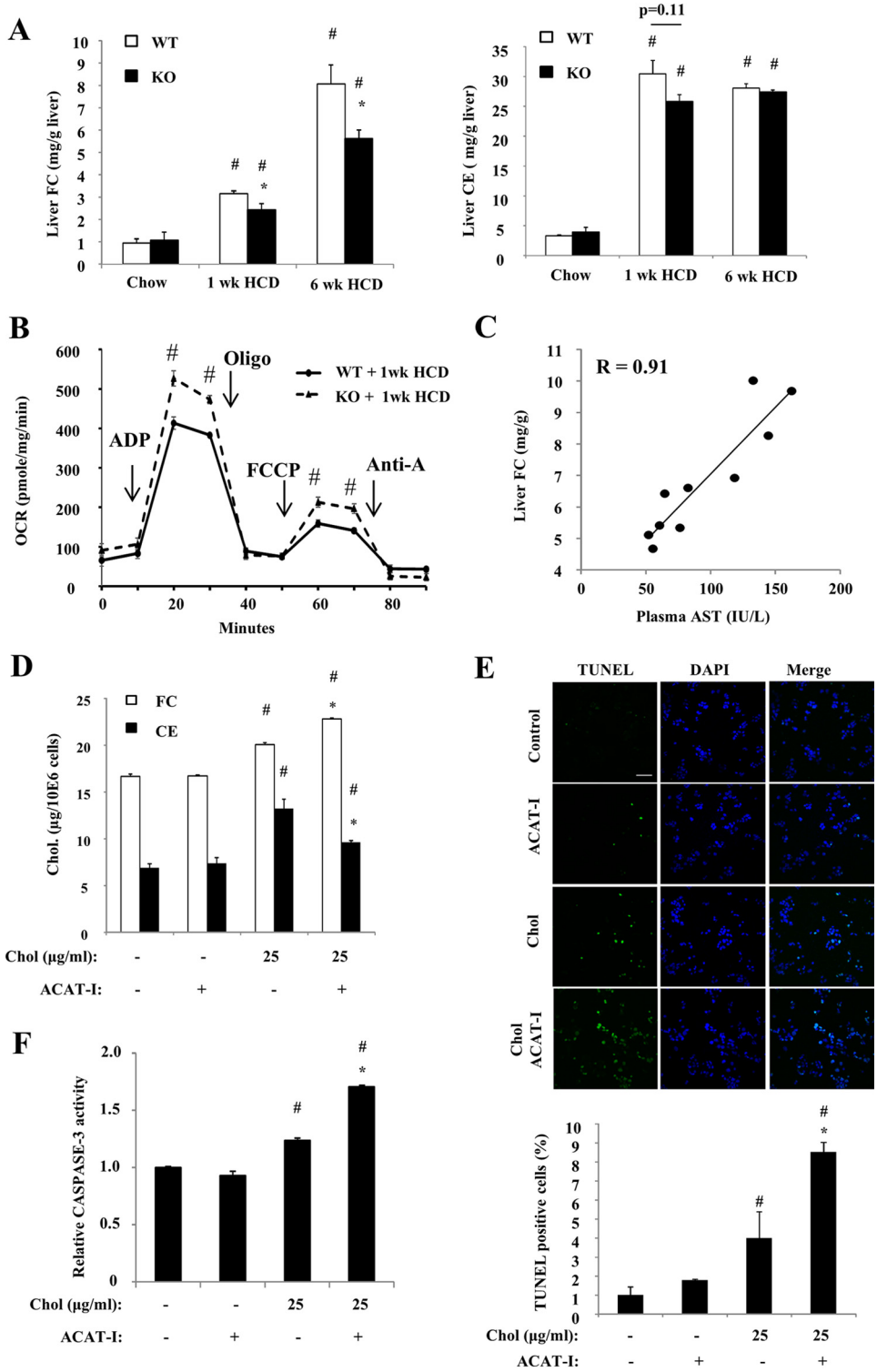

FIGURE 2. **HCD-fed *Sort1* KO mice accumulated less cholesterol in the liver.** WT and *Sort1* KO mice were fed a chow diet or an HCD for 1 week or 6 weeks. Mice were fasted overnight before sacrifice. *A*, liver FC and CE levels. $n = 4–6$. * indicates statistical significance, *versus* WT mice on same diet. # indicates statistical significance, *versus* chow-fed mice of the same genotype. *B*, analysis of bioenergetics function of freshly isolated liver mitochondria with a Seahorse XF analyzer. Pooled liver mitochondria from 4–6 mice were used. Assays were done in triplicates and expressed as mean ± S.D. # indicates statistical significance, *versus* WT mice. *Oligo*, oligonucleotide; *FCCP*, carbonyl cyanide *p*-trifluoromethoxyphenylhydrazone; *OCR*, oxygen consumption rate; Anti-A, Antimycin A. *C*, correlation between liver FC and plasma AST. *D–F*, HepG2 cells were treated with cholesterol (*Chol.*, complexed to methyl-β-cyclodextrin) and/or ACAT inhibitor (*ACAT-I*, 12.5 μg/ml) for 16 h as indicated. *D*, cholesterol assays were repeated in triplicates. *E*, TUNEL-positive cells were counted in 3 independent experiments (a total of ~1000 cells/group were counted). *Scale bar*: 50 μm. *F*, caspase-3 activity assays were repeated in triplicates. Results in *D–F* are expressed as mean ± S.D. # indicates statistical significance, *versus* untreated controls. * indicates statistical significance, *versus* cholesterol-treated cells (*third column*).

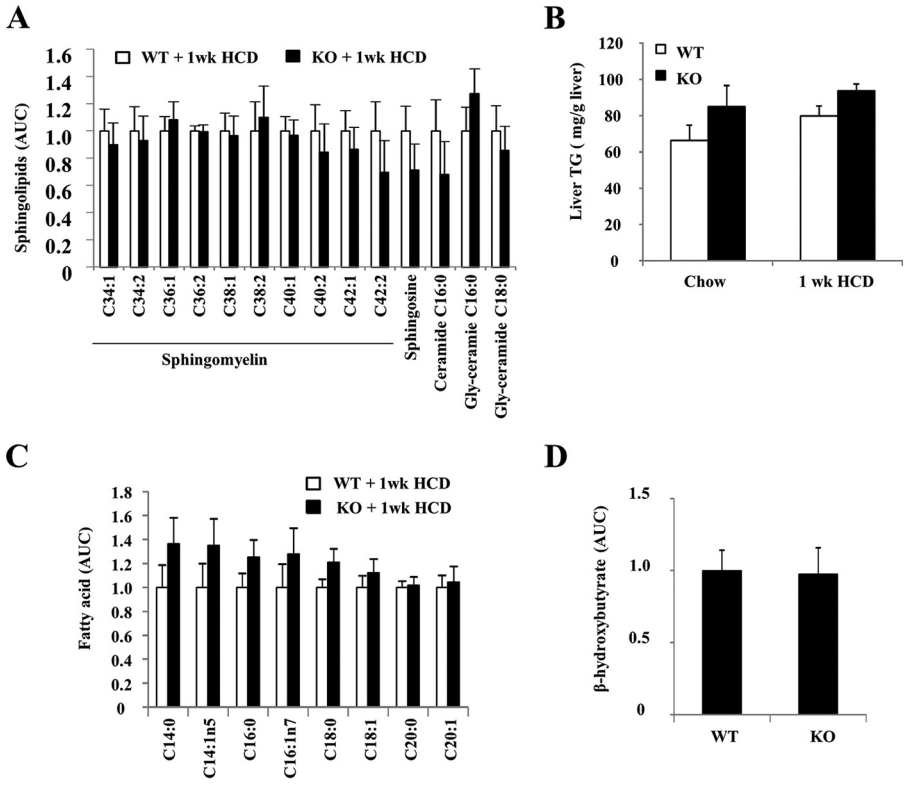

FIGURE 3. **Hepatic sphingolipids and fatty acids in WT and *Sort1* KO mice.** *A*, *C*, and *D*, livers of 1-week HCD-fed mice were used for metabolomics analysis of sphingolipids (*A*), fatty acids (*C*), and ketone body β-hydroxybutyrate levels (*D*). *AUC*, area under the curve. *B*, hepatic triglyceride (*TG*) was measured with an assay kit. All results are expressed as mean ± S.E. $n = 5–6$.

mice had significantly reduced biliary cholesterol output but similar bile acid and phospholipid output when compared with WT mice (Fig. 4*D*). Furthermore, fecal cholesterol excretion was similar between WT and *Sort1* KO mice (Fig. 4*E*). Taken together, these data suggest that reduced hepatic FC accumulation in *Sort1* KO mice was not due to higher biliary and fecal cholesterol excretion. On the contrary, lower hepatic cholesterol accumulation likely decreased biliary cholesterol output and prevented gallstone formation in *Sort1* KO mice.

HCD-fed Sort1 KO Mice Showed Increased Hepatic Bile Acid Synthesis—Cholesterol conversion into bile acid is the most quantitatively significant pathway for cholesterol catabolism in the liver. Hepatic CYP7A1 (cholesterol 7α-hydroxylase) and CYP8B1 (sterol 12α-hydroxylase) mRNA levels were similar between WT and *Sort1* KO mice under chow-fed conditions (Fig. 5*A*). HCD feeding significantly decreased CYP7A1 and CYP8B1 mRNA in WT mice. However, CYP7A1 was repressed to a much lesser extent in *Sort1* KO mice, resulting in much higher CYP7A1 mRNA expression in HCD-fed *Sort1* KO mice (Fig. 5*A*). Due to an unknown mechanism, hepatic SHP mRNA was higher in *Sort1* KO mice under the chow condition (Fig. 5*A*), but this increase of SHP mRNA did not correlate with lower hepatic CYP7A1 in chow-fed *Sort1* KO mice. Under the HCD-fed condition, expression of hepatic SHP and ileum fibroblast growth factor 15 (FGF15) was similar in WT and *Sort1* KO mice (Fig. 5, *A* and *B*), suggesting that higher CYP7A1 expression in HCD-fed *Sort1* KO mice may not be due to altered FXR signaling. Because higher CYP7A1 expression may indicate higher *de novo* bile acid synthesis, we analyzed hepatic bile acids in these mice. HCD-fed *Sort1* KO mice had higher levels of tauro-conjugated and free chenodeoxycholic acid (CDCA), muricholic acid (MCA), and ursodeoxycholic acid (UDCA) in the liver (Fig. 5, *C* and *D*). Consistently, analysis of bile acid composition in the bile showed that HCD-fed *Sort1* KO mice had a significantly increased percentage of CDCA and MCA when compared with that of HCD-fed WT mice (Fig. 5*E*). Furthermore, the level of 7α-HO-3-oxo-4-cholestenoate, an intermediate in the acidic bile acid synthetic pathway, was ~5-fold higher in *Sort1* KO mice over WT controls (Fig. 5*F*), suggesting that hepatic bile acid synthesis through the acidic pathway also markedly increased in *Sort1* KO mice, although the mRNA of CYP27A1 (sterol 27-hydroxylase), which catalyzes the first and rate-limiting step in the acidic pathway, was not higher in these mice (Fig. 5*A*). Although the classic bile acid synthesis pathway produces both CA and CDCA, the acidic pathway mainly produces CDCA, the majority of which is converted to MCAs and also UDCA in mice. Therefore, stimulation of the acidic pathway provides a possible explanation for higher levels of conjugated and free CDCA, MCAs, and UDCA, as well as a possibly more hydrophilic bile acid pool in the livers of HCD-fed *Sort1* KO mice. In mice, the acidic pathway may contribute significantly to overall hepatic bile acid synthesis (34), and stimulation of this pathway may further contribute to decreased hepatic FC accumulation.

Identification of Functional SORT1-CES1 Interaction—Given that the molecular basis underlying the altered hepatic cholesterol and bile acid metabolism in *Sort1* KO mice is still not clear, we reasoned that using an unbiased approach to iden-

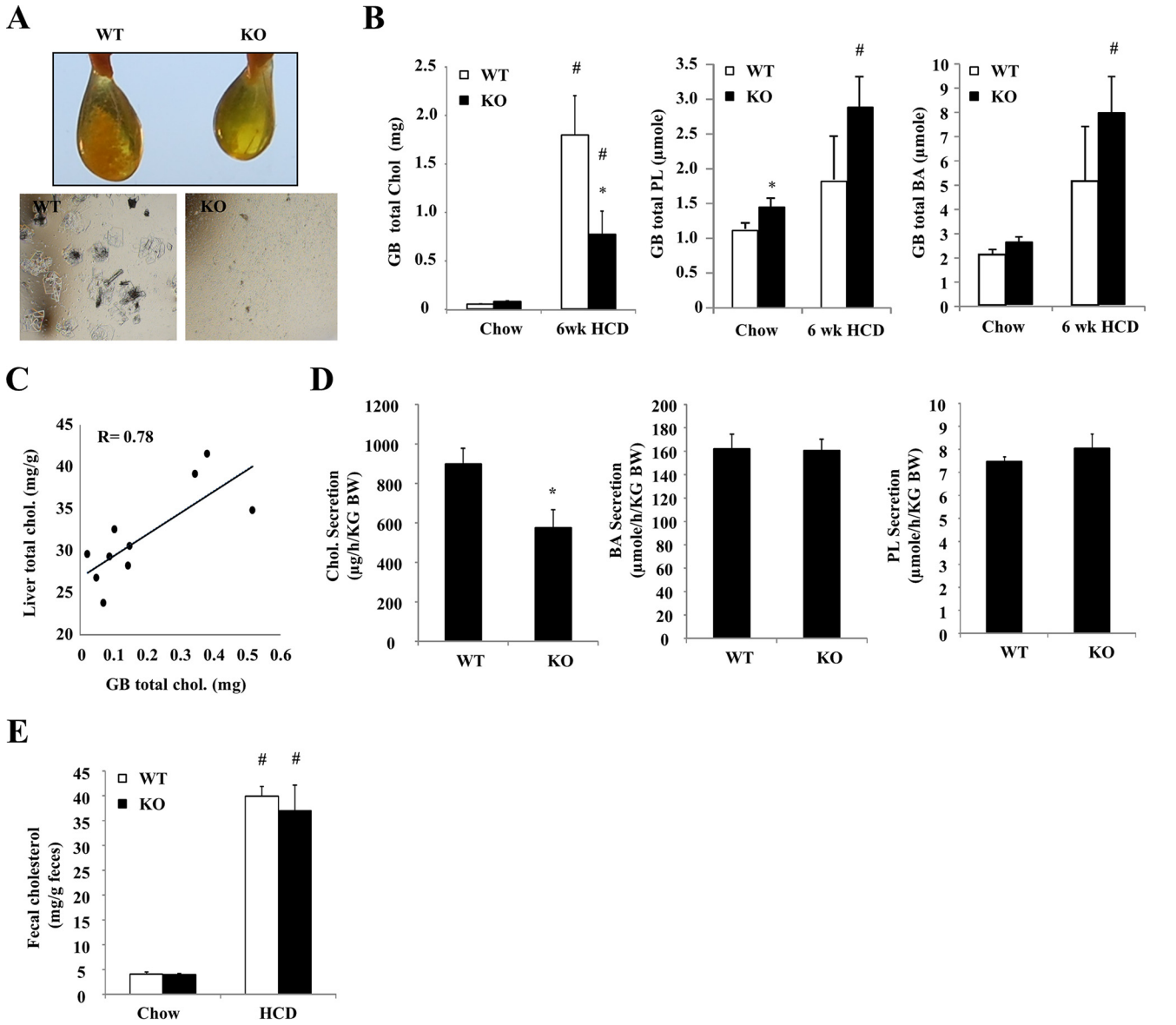

FIGURE 4. **HCD-fed *Sort1* KO mice had decreased biliary cholesterol secretion and were protected against gallstone formation.** *A*, gallbladder appearance and microscopic detection of crystal in the bile of 6-week HCD-fed WT and *Sort1* KO mice. *B*, gallbladder (*GB*) cholesterol (*Chol*), phosphatidylcholine (*PL*), and bile acid (*BA*) levels. $n = 4–6$. *C*, correlation between liver total cholesterol and gallbladder cholesterol in 6-week HCD-fed WT and *Sort1* KO mice. $n = 4–6$. *D*, WT and *Sort1* KO mice were fed an HCD for 1 week. Mice were fasted overnight, and bile was collected via cannulation for 60 min as described under "Experimental Procedures." $n = 6–7$. *E*, mice were fed HCD for 1 week, and feces were collected over the last 3-day period. All results are expressed as mean ± S.E. * indicates statistical significance, *versus* WT mice on same diet. # indicates statistical significance, *versus* chow-fed mice of the same genotype.

tify SORT1-interacting proteins may help reveal novel SORT1-regulated pathways in the liver. To this end, ectopically expressed FLAG-tagged human SORT1 and its interacting proteins were co-immunoprecipitated in HepG2 cell lysate (Fig. 6*A*) or mouse liver lysate (not shown) and subjected to LC-MS/MS-based proteomics analysis. Many identified proteins are known SORT1 ligands such as apolipoprotein-B100 (ApoB100) (3, 6), cathepsins (2), or proteins involved in vesicle trafficking such as GGA2 (Golgi-localized, γ adaptin ear-containing, ARF-binding 2) and Rab proteins (Table 1), which thus validated this approach. CES1, which was shown to protect against cellular cholesterol and triglyceride accumulation and inflammation (22–24, 35), was identified as a SORT1-interacting protein in both HepG2 cells and mouse livers (Table 1). The SORT1-CES1 interaction was further confirmed with independent co-immunoprecipitates (co-IP) using HepG2 lysates (Fig. 6*B*). With validated antibodies (Fig. 6*C*), we confirmed that SORT1 interacted with mouse CES1 (also known as Es-X), but not CES3 (also known as triacylglycerol hydrolase (TGH)), which shares overlapping function and some degree of sequence homology with CES1 (Fig. 6*D*). To determine whether and how SORT1 regulates CES1, we knocked down SORT1 in HepG2 cells, which increased CES1 protein without altering CES1 mRNA (Fig. 6, *E* and *F*). Furthermore, liver CES1 protein, but not mRNA, was ~2-fold higher in *Sort1* KO mice than WT mice (Fig. 6, *G* and *H*). Liver CES3 protein levels were similar in WT and *Sort1* KO mice (Fig. 6*G*).

It is well established that SORT1 delivers many of its protein ligands to the late endosomes/lysosomes for degradation (2, 3). We therefore hypothesize that SORT1 may mediate lysosome

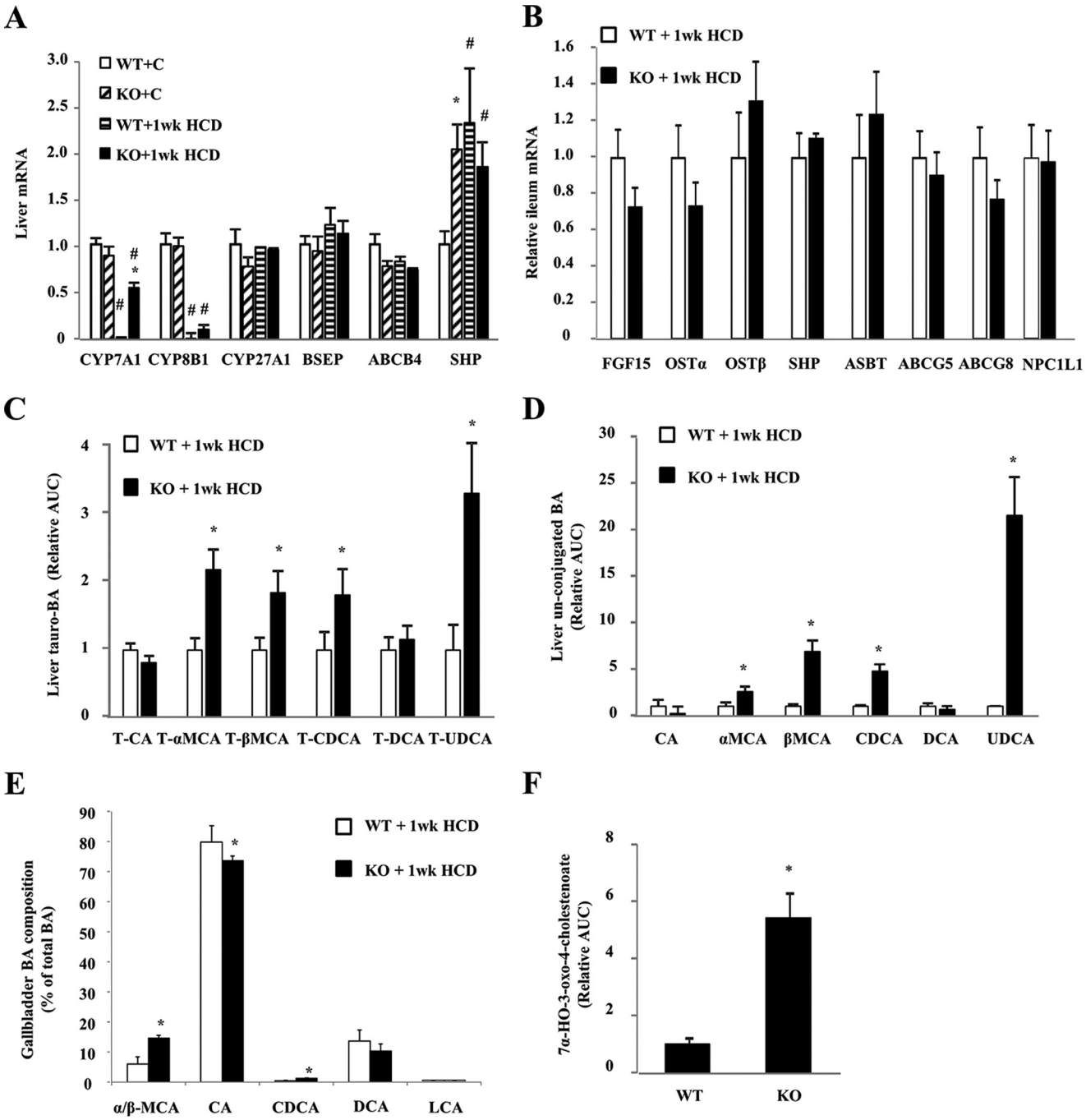

FIGURE 5. **HCD-fed *Sort1* KO mice had increase bile acid synthesis and altered bile acid composition.** Tissues of 1-week HCD-fed mice were used for analysis. *A*, liver mRNA levels. *B*, ileum mRNA expression. *WT+C*, WT plus chow diet; *KO+C*, knock-out plus chow diet. *C* and *D*, hepatic taurine-conjugated and free bile acids (*BA*) determined by metabolomics analysis. Values in WT mice were set as 1. *AUC*, area under the curve; *T*, total. *E*, bile acid composition in gallbladder bile was analyzed by LC-MS/MS. *F*, liver 7α-HO-3-oxo-4-cholestenoate detected by metabolomics analysis. The value in WT was set as 1. All results are expressed as mean ± S.E. $n = 5–6$. * indicates statistical significance, *versus* WT mice on same diet. # indicates statistical significance, *versus* chow-fed mice of the same genotype.

targeting of CES1, which explains why SORT1 deficiency increased CES1 abundance. To test this hypothesis, we next studied SORT1 and CES1 cellular localization in HepG2 cells. Although it is well established that SORT1 is targeted to late endocytic compartments, we consistently found that SORT1 showed predominantly perinuclear localization with significant co-localization with the Golgi marker TGN46 and minimal co-localization with late endosome/lysosome marker Lamp1 in untreated HepG2 cells (Fig. 7, *A* and *B*) and mouse liver AML12 cells (36). This is not unexpected because it is well known that SORT1 rapidly retrograde traffics back to the TGN in the retromer complex after "unloading" its ligands in the acidic environment of the late endocytic compartments (37). Because such rapid SORT1 retrograde trafficking made it difficult to study SORT1 endosome localization under basal culture conditions, we subjected HepG2 cells to short term (3-h) amino acid starvation (−AA) plus chloroquine (CQ) treatment, which increased lysosome numbers and simultaneously raised late

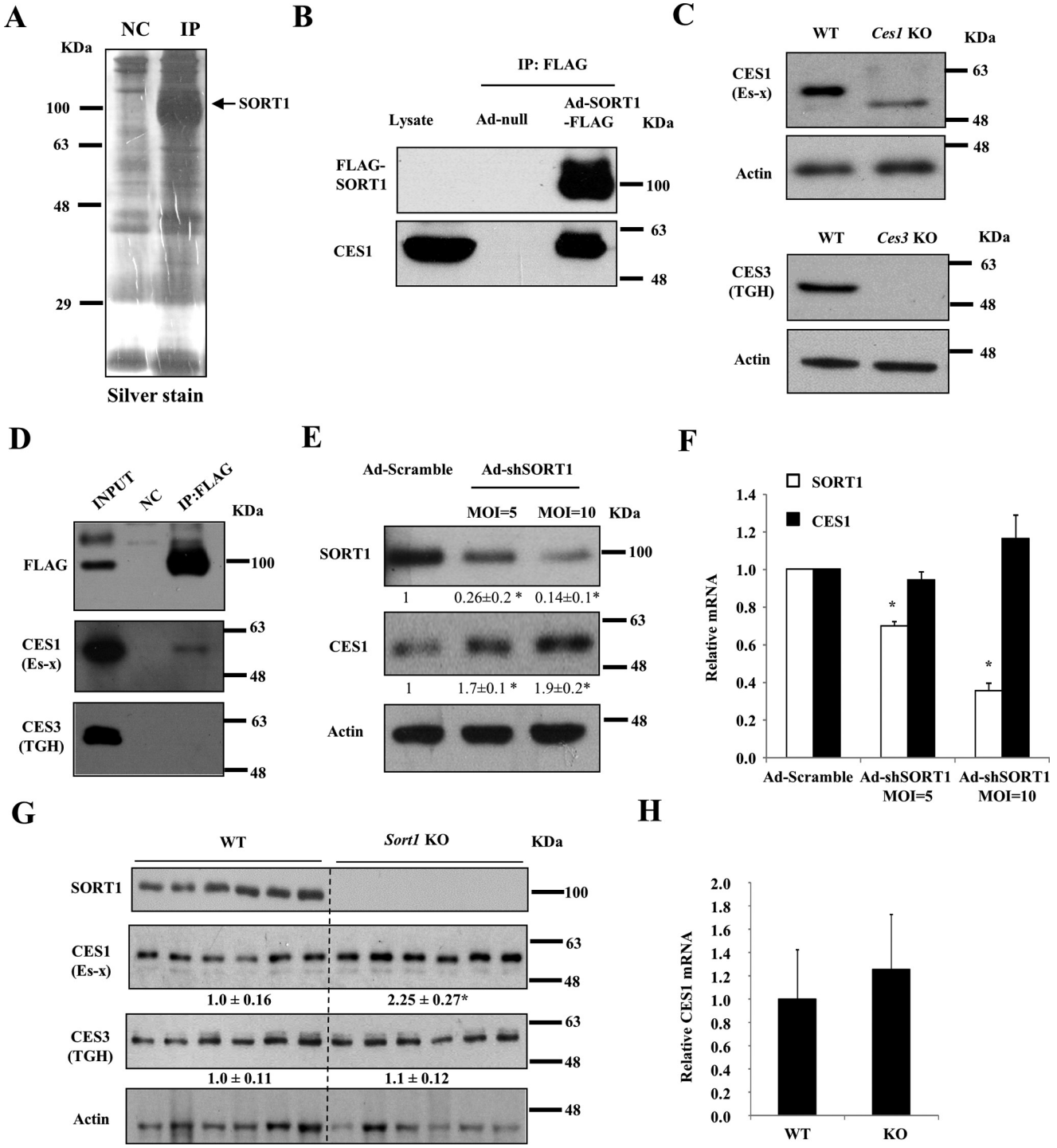

FIGURE 6. **Identification of functional interaction of SORT1 and CES1 in HepG2 cells and mouse livers.** *A*, HepG2 cells were infected with Ad-null or Ad-SORT1-FLAG at an MOI of 1 for 16 h. Cell lysate was used for immunoprecipitation with anti-FLAG antibody conjugated to magnetic beads. Immunoprecipitates were subjected to SDS-PAGE and silver staining before being submitted for proteomics analysis. *NC*, negative control. *B*, HepG2 cells were infected with Ad-null or Ad-SORT1-FLAG at an MOI of 1 for 16 h. Cell lysate was used for immunoprecipitation with anti-FLAG antibody conjugated to magnetic beads. SORT1-FLAG was detected with anti-FLAG antibody. Non-infected HepG2 cell lysate was used to detect CES1 band as controls. This experiment was performed three times, and all experiments showed CES1 co-precipitation with SORT1. *C*, validation of CES1 and CES3 antibodies with liver lysate from *Ces1* and *Ces3* knock-out mice. *TGH*, triacylglycerol hydrolase. *D*, immunoprecipitation of SORT1 from mouse livers expressing SORT1-FLAG followed by Western blotting analysis. Mice were injected with Ad-null. This experiment was repeated three times, and CES1 was co-precipitated with SORT1 in all experiments. *E* and *F*, HepG2 cells were infected with Ad-shSORT1 at an MOI of 5 or 10 for 24 h. Ad-scramble was used to infect control cells. In *E*, Western blotting was performed to detect SORT1 and CES1 protein. Average band intensity of 3 independent experiments (normalized to actin) was shown as values below the blot. In *F*, real-time PCR was used to measure CES1 and SORT1 mRNA in three experiments. Results are expressed as mean ± S.D. * indicates statistical significance, *versus* Ad-siCon. *G* and *H*, liver protein and mRNA of WT and *Sort1* KO mice on chow diet. Values below the blot indicate the relative band intensity (normalized to actin) in each group. Results are expressed as mean ± S.E. * indicates statistical significance, *versus* WT mice. $n = 6$.

TABLE 1
LC-MS/MS identification of Sort1-interacting proteins
NC, negative control; SpC, spectra count; ND, not detected.

	HepG2 cells		Mouse livers	
Protein ID	NC (SpC)	IP (SpC)	NC (SpC)	IP (SpC)
Sortilin 1	9	2405	17	737
CES1	0	55	0	4
ApoB100	0	119	ND	ND
GGA2	0	12	0	10
Tubulin α	0	35	0	28
Rab9	ND	ND	0	5
Rab14	0	5	0	4
Rab21	0	8	ND	ND
Cathepsin B	0	3	ND	ND
Cathepsin D	ND	ND	0	4

endosome/lysosome pH and impaired their function. This treatment rapidly and almost completely abolished the perinuclear localization of SORT1 and caused dispersed distribution of SORT1-positive puncta throughout the cells (Fig. 7, *A* and *B*). A significant number of these SORT1-positive puncta co-localized with Lamp1 (yellow puncta indicated by *white arrows* in Fig. 7*B*), suggesting that these puncta likely represented SORT1 on the late endocytic compartments. Some SORT1-positive puncta did not co-localize with Lamp1 (green puncta indicated as *red arrows* in Fig. 7*B*), which may represent SORT1-containing trafficking vesicles before fusing with impaired late endocytic compartments. These results also implied that SORT1 dynamically traffics between the late endocytic compartments and Golgi at a high rate, which is invisible under basal culture conditions. Next, confocal microscope analysis under these experimental conditions showed substantial SORT1-CES1 co-localization in the perinuclear region in untreated cells, whereas CES1 co-localized to SORT1-positive puncta in −AA/CQ-treated cells (indicated by *white arrows* in Fig. 7*C*). These results were further confirmed with high resolution stimulated emission depletion (STED) microscopy (Fig. 7*D*). These results suggest that SORT1 may interact with CES1 in trafficking vesicles that are targeted to late endocytic compartments.

Knockdown of Hepatic CES1 Increased HCD-induced Liver Injury and Abolished the Protective Effect in Sort1 KO Mice—We next reasoned that if higher CES1 indeed protects against HCD-induced liver injury, liver CES1 deficiency would exacerbate HCD-induced liver injury in mice. To test this, we acutely knocked down hepatic CES1 in WT and *Sort1* KO mice with Ad-shCES1 injection (Fig. 8*A*). One week after injection, we fed mice an HCD for one additional week, and liver injury was studied. In Ad-scramble-injected control groups, *Sort1* KO mice had significantly lower plasma AST and ALT than WT as expected (Fig. 8*B*). Ad-shCES1-injected WT and *Sort1* KO mice showed markedly higher elevation of AST and ALT levels upon HCD challenge, and no differences were observed between WT and *Sort1* KO mice fed an HCD (Fig. 8*B*). Consistently, livers of Ad-shCES1-injected WT and *Sort1* KO mice showed more severe histological features of hepatocyte injury and hydropic degeneration than the Ad-scramble-injected mice (Fig. 8*C*). Consistent with our earlier observation shown in Fig. 1*E*, only MCP1 mRNA was significantly lower in *Sort1* KO mice after 1 week of HCD feeding (Fig. 8*D*). Furthermore, 1 week of HCD significantly induced MCP1 and TNFα mRNA when CES1 was knocked down in mice (Fig. 8, *D* and *E*). These results suggest that liver CES1 knockdown exacerbated HCD-induced liver injury and abolished the protective effects in *Sort1* KO mice.

Measurement of hepatic cholesterol levels showed that Ad-scramble-injected *Sort1* KO mice accumulated less FC than WT controls (Fig. 9*A*), which was similar to the results shown in Fig. 2*A*. Unexpectedly, knockdown of hepatic CES1 did not cause further increase of hepatic FC or CE accumulation, but markedly increased plasma cholesterol levels (Fig. 9, *A*–*D*). In Ad-scramble-injected mice, gallbladder cholesterol was significantly lower in *Sort1* KO mice (Fig. 9*E*), which was consistent with data shown in Fig. 4*B*. CES1 knockdown also significantly decreased gallbladder cholesterol in WT mice but not *Sort1* KO mice (Fig. 9*E*). The hepatic LDLR protein abundance was not significantly different between the four groups (Fig. 9*F*). Fig. 9*G* shows that hepatic CES1 knockdown mainly increased the cholesterol in VLDL and HDL fractions, although the LDL cholesterol also seemed to be modestly increased upon CES1 knockdown. It should be noted that unlike humans, mice have relatively low levels of plasma LDL cholesterol. Because VLDL particles are directly produced by the liver and they usually contain very low levels of cholesterol, the markedly elevated VLDL cholesterol suggests increased hepatic cholesterol secretion. These results collectively suggest that hepatic CES1 knockdown significantly increased the susceptibility to HCD-induced liver injury and inflammation, and abolished the protection in *Sort1* KO mice. Furthermore, although increased CES1 can reduce hepatic cholesterol, CES1-deficient livers may respond to HCD challenge by secreting cholesterol into the blood circulation, resulting in hypercholesterolemia.

Discussion

Despite the recently identified association of *SORT1* gene to cholesterol homeostasis in humans by genome-wide association studies, the role and mechanism of liver SORT1 in the regulation of cholesterol homeostasis are still incompletely understood. In this study, we provided *in vitro* and *in vivo* evidence to show that SORT1 deficiency caused increased CES1 protein abundance and that SORT1 and CES1 co-localized in trafficking vesicles in HepG2 cells. Given the well documented role of SORT1 in mediating the lysosome targeting and degradation of its protein cargos (1–3), our results support the hypothesis that SORT1 mediates lysosome CES1 targeting and degradation, and SORT1 loss of function resulted in higher liver CES1. Upon an HCD challenge, *Sort1* KO mice showed less hepatic FC accumulation and significantly attenuated liver injury and inflammation, which was consistent with the previously reported role of liver CES1 in protecting against cellular cholesterol accumulation and injury (22–24, 35). Therefore, this study revealed a novel SORT1-CES1 axis that modulates hepatic cholesterol metabolism in mice and further suggested that therapeutic inhibition of hepatic SORT1 may be beneficial in improving hepatic cholesterol homeostasis in liver diseases.

A number of previous studies have suggested that higher liver CES1 expression may cause further downstream metabolic changes that enhance hepatic cholesterol export or catabolism. Hepatocyte CES1 overexpression directly promoted

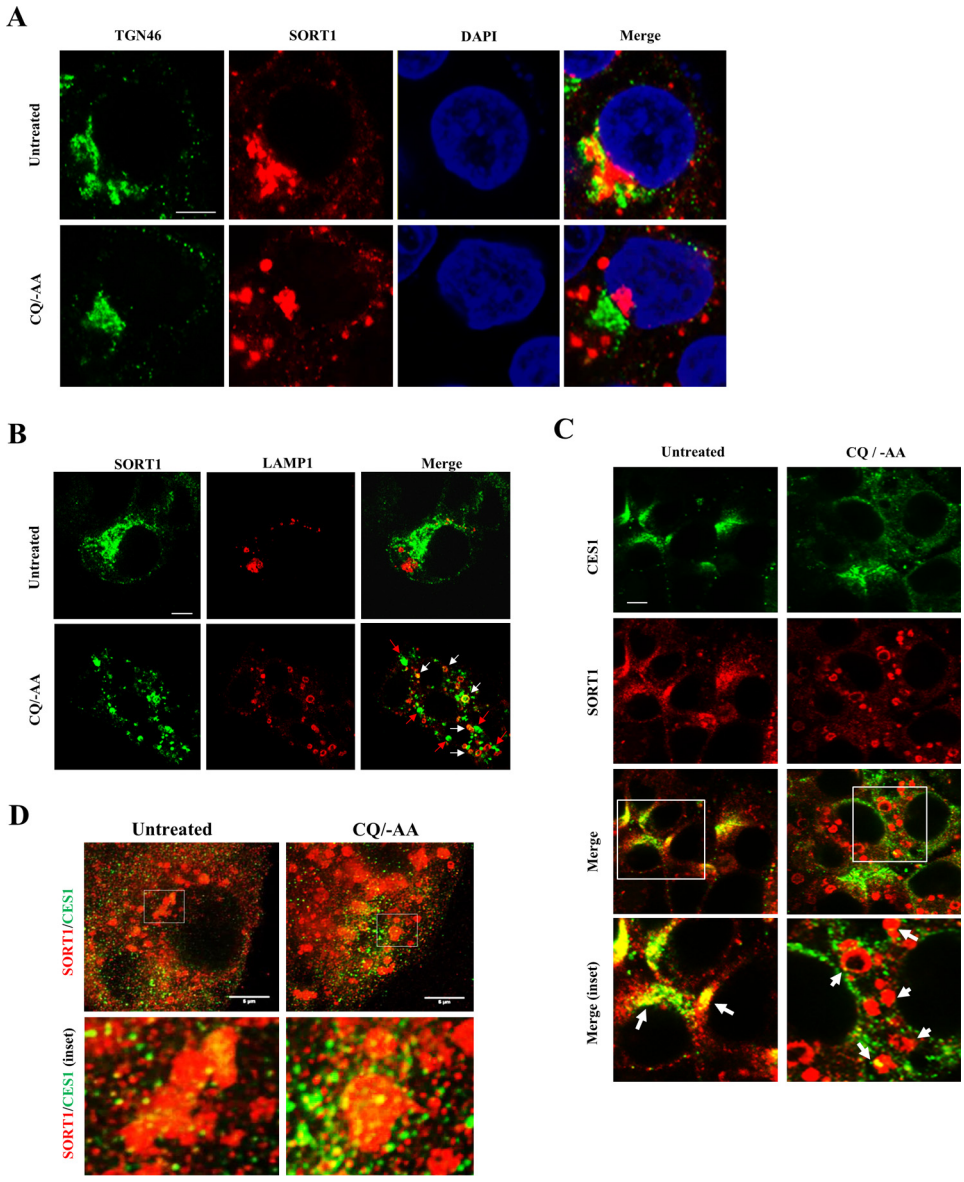

FIGURE 7. **SORT1 and CES1 co-localization in HepG2 cells.** HepG2 cells were cultured under basal condition or treated with CQ (25 μM) in amino acid-free Earle's balanced salt solution medium for 3 h. *A–C*, confocal microscope images. *Scale bar*: 5 μm. *D*, STED microscope images. *Scale bar*: 5 μm.

cholesterol conversion into bile acids (20, 23, 26, 38). To understand the initial response to HCD challenge at an early time point that accounted for the protective effects after chronic HCD challenge in *Sort1* KO mice, we studied biliary cholesterol secretion and bile acid synthesis in 1-week HCD-fed mice. Results from these experiments suggested that increased bile acid synthesis, but not higher biliary cholesterol secretion, may be responsible for lowered hepatic FC accumulation. This is supported by elevated levels of many bile acid species in the liver of HCD-fed *Sort1* KO mice, especially unconjugated bile acids, a significant portion of which may be from *de novo* bile acid synthesis in the liver. Several mechanisms may be responsible for higher bile acid synthesis in HCD-fed *Sort1* KO mice. In addition to the reported CES1 effect on stimulating liver bile acid synthesis by producing FC as the substrate, HCD-fed *Sort1* KO mice also had higher CYP7A1 expression than WT controls. Dietary cholate contained in the HCD can repress hepatic CYP7A1 expression via FXR signaling in the liver and the intestine. However, the higher CYP7A1 in HCD-fed *Sort1* KO mice was not likely due to altered FXR signaling because liver SHP and intestine FGF15 expression was similar in HCD-fed *Sort1* KO mice and WT controls (Fig. 5, *A* and *B*). On the other hand, cholesterol feeding has also been shown to repress CYP7A1 in mice, likely due to liver inflammatory response (39, 40). Higher CYP7A1 in *Sort1* KO mice correlated with lower liver FC accumulation and attenuated liver injury. Interestingly, our analysis of liver metabolites revealed an ~5-fold increase of 7α-HO-3-oxo-4-cholestenoate in *Sort1* KO mice, suggesting strong stimulation of the acidic bile acid synthesis pathway in the absence of hepatic CYP27A1 induction. As previously suggested by studies in CES1-overexpressing mice (20, 26), this may be driven by increased substrate feeding into the bile acid synthetic pathway. Increased bile acid synthesis via the acidic pathway cannot only contribute to decreased hepatic FC accumula-

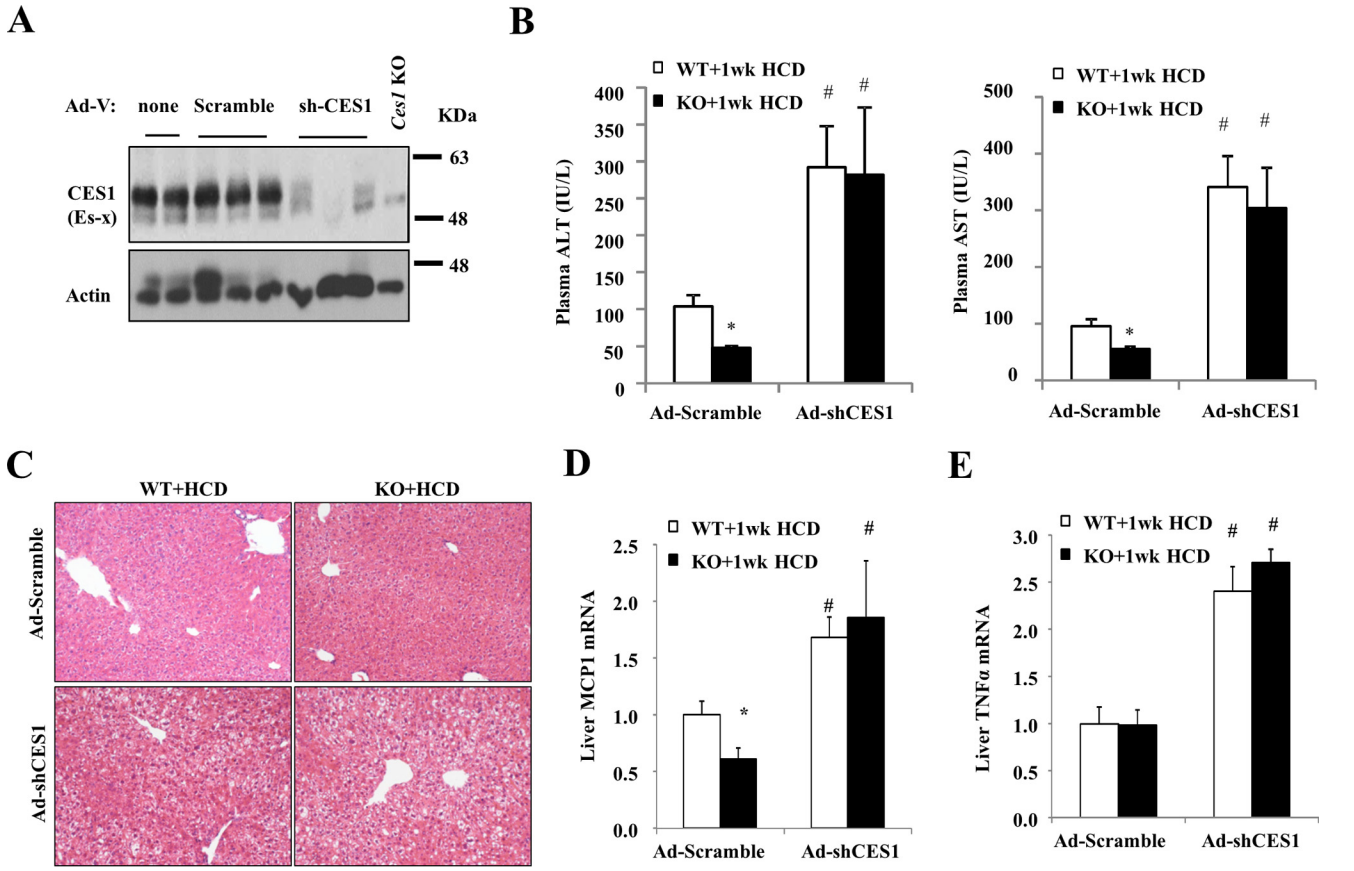

FIGURE 8. **Hepatic CES1 knockdown exacerbated liver injury and abolished the protective effects in HCD-fed *Sort1* KO mice.** WT and *Sort1* KO mice were injected with Ad-scramble or Ad-shCES1. One week later, mice were challenged with HCD for one additional week. Mice were fasted overnight before sacrifice. *A*, Western blot to show knockdown efficiency. Liver lysate from *Ces1* KO mice was used as control. *B*, plasma ALT and AST. *C*, H&E staining of liver sections. *D* and *E*, hepatic cytokine mRNA expression. All results are expressed as mean ± S.E. $n = 5–7$. * indicates statistical significance, *versus* WT mice injected with same adenovirus vector. # indicates statistical significance, *versus* Ad-scramble-injected mice of the same genotype.

tion, this may also provide a possible explanation of increased hydrophilic bile acid MCA and UDCA in the bile acid pool.

In this study, we acutely knocked down hepatic CES1 to determine the role of CES1 in the protection against cholesterol lipotoxicity in *Sort1* KO mice. These studies supported a critical role of CES1 in the protection against HCD-induced hepatic injury in mice, because mice deficient in CES1 showed increased susceptibility to HCD-induced liver injury and inflammation. Interestingly, these experiments also revealed that CES1 knockdown did not cause intrahepatic cholesterol accumulation, but rather increased plasma cholesterol levels. These results suggest that CES1 gain-of-function and loss-of-function do not necessarily produce completely opposite changes of intracellular cholesterol metabolism. When liver CES1 expression is increased, CES1 can direct cholesterol into the bile acid synthesis pathway for elimination (20, 23, 26, 38). On the other hand, once hepatic CES1 is reduced, hepatocytes may instead secrete excessive cholesterol into the blood circulation as an adaptive response. This is consistent with liver's ability to tightly control intracellular cholesterol homeostasis via fine-tuning multiple input and output pathways as an adaptive response. Nevertheless, it is somewhat puzzling that liver CES1 knockdown still markedly increased susceptibility to injury without increasing total liver cholesterol. One possibility may lie in the effect on the intracellular FC and CE interconversion. It is well known that cellular cholesterol undergoes continuous cycles of CE hydrolysis and FC re-esterification even under basal conditions, a process that plays a critical role in regulating intracellular cholesterol trafficking and organelle cholesterol homeostasis (41). We showed here that either inhibition of ACAT in HepG2 cells or knockdown of CES1 in mouse livers exacerbated cholesterol-induced cell injury, suggesting that disruption of intracellular FC and CE interconversion in either direction may increase the susceptibility to cholesterol toxicity especially under cholesterol overloading conditions. It is possible that disruption of FC and CE interconversion has a significant negative impact on the cell's ability to maintain organelle cholesterol homeostasis, but such changes may not be reflected at whole cell cholesterol levels. Nevertheless, this hypothesis needs to be further substantiated by additional experimental evidence from future investigations.

Here we mainly focused this study on the role of the SORT1-CES1 axis in the regulation of hepatic cholesterol metabolism because of the recently identified link between *SORT1* and cholesterol levels in humans (4, 5). On the other hand, many studies also showed that CES1-dependent fatty acid mobilization prevented hepatic fat accumulation in mice (21, 22, 24, 35). A more recent study reported that *Sort1* KO mice were protected against high fat diet-induced obesity and fatty liver, which was attributed to reduced ceramide production and signaling (33).

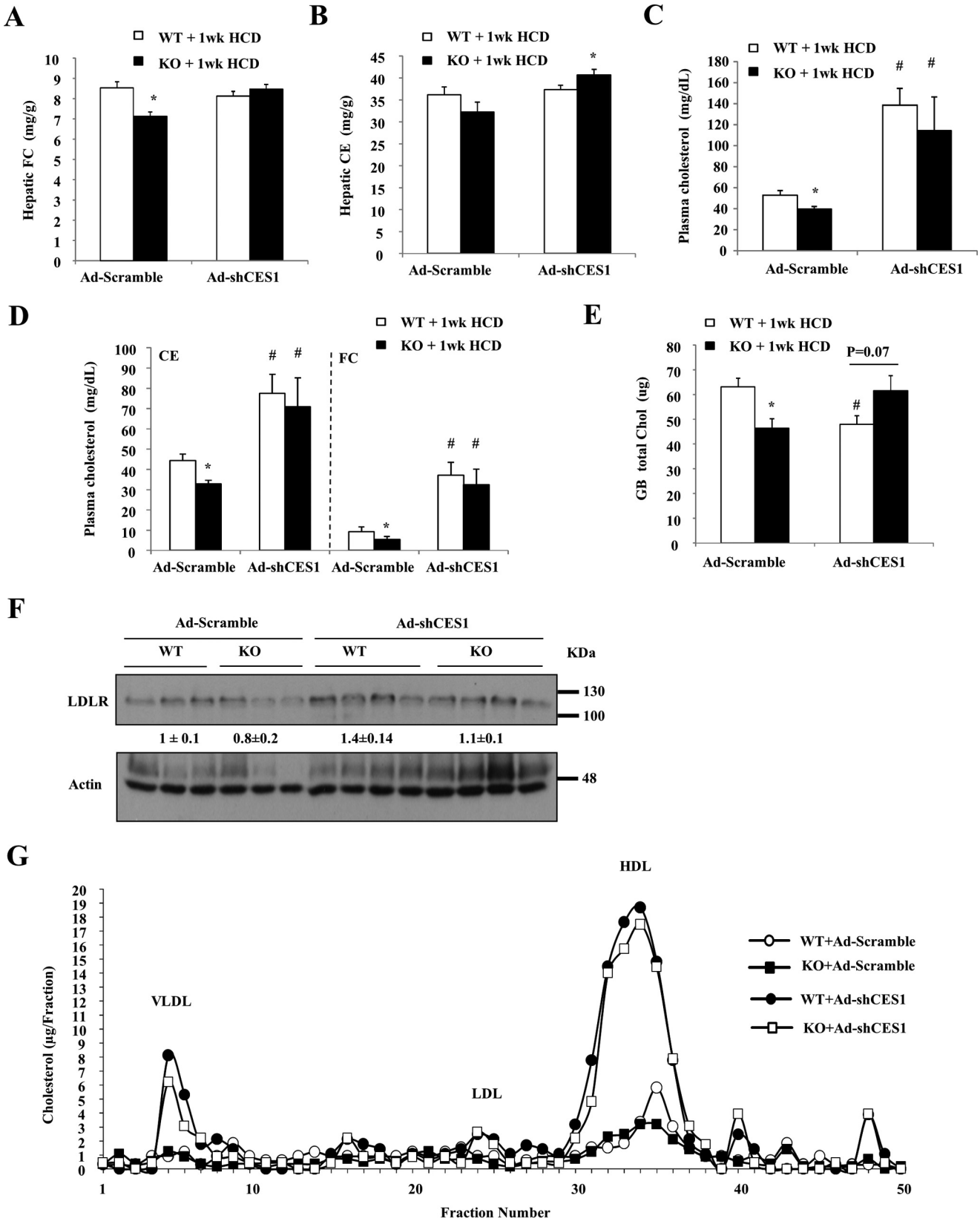

FIGURE 9. **Hepatic CES1 knockdown increased plasma cholesterol levels without altering hepatic cholesterol accumulation in mice.** The same samples as described in Fig. 8 were used for the analysis. *A* and *B*, hepatic cholesterol levels. *C* and *D*, plasma total cholesterol, CE, and FC levels. *E*, gallbladder total cholesterol (*GB total Chol*). *F*, hepatic LDLR protein. Band intensity (normalized to actin) was expressed as mean ± S.E. *G*, pooled plasma ($n = 5–7$) was used for determination of lipoprotein profile. All results (except *G*) are expressed as mean ± S.E. $n = 5–7$. * indicates statistical significance, *versus* WT mice injected with same adenovirus vector. # indicates statistical significance, *versus* Ad-scramble-injected mice of the same genotype.

In our experimental model, we did not observe altered hepatic sphingolipids in *Sort1* KO mice. Whether the SORT1-CES1 axis plays a role in attenuating high fat diet-induced hepatic triglyceride accumulation is currently under investigation.

Taken together, this study identified a functional SORT1-CES1 axis in the liver, and thus improved current understanding of the mechanistic link between SORT1 function and cholesterol metabolism. Based on results from this study, therapeutic approaches that inhibit hepatic SORT1 function may be beneficial in attenuating hepatic cholesterol accumulation and cholesterol lipotoxicity.

Experimental Procedures

Reagents—Anti-SORT1 rabbit IgG (ab16640), anti-human CES1 (ab45957), anti-CES2 (ab137606), and anti-TGN46 (ab16059) antibodies were purchased from Abcam (Cambridge, MA). Anti-mouse CES1 (AF7929), anti-SORT1 goat IgG (AF3154), and anti-LDLR (MAB2255) were purchased from R&D Systems (Minneapolis, MN). Actin antibody, chloroquine, and caspase-3 assay reagents were purchased from Sigma. F4/80 antibody was purchased from Bio-Rad. Anti-Lamp1 antibody was purchased from the Developmental Studies Hybridoma Bank (DSHB) at the University of Iowa. Alexa Fluor 488 IgG and Alexa Fluor 594 were purchased from Life Technologies. HepG2 cells were purchased from ATCC (Manassas, VA). AST and ALT assay kits, a total cholesterol assay kit, and a triglyceride assay kit were purchased from Pointe Scientific (Canton. MI). A free cholesterol assay kit was purchased from Wako Diagnostics (Richmond, VA). A bile acid assay kit was purchased from Diazyme Laboratories (Poway, CA). A phosphatidylcholine assay kit was purchased from BioVision (Milpitas, CA). A TUNEL assay kit was purchased from Roche Applied Science.

Mice—Global *Sort1* KO mice were obtained from Taconic Biosciences Inc. The *Sort1* gene (accession number: NM_019972) was silenced by inserting a stop codon into the second intron of the *Sort1* gene through gene trapping technology. Mice on a 129/SvEv/C57BL/6 mixed background were backcrossed to C57BL/6J (The Jackson Laboratory) for more than seven generations before aged-matched *Sort1* KO and WT mice were generated for the use in this study. Mice were housed in micro-isolator cages with corn cob bedding under a normal light-dark cycle. Experiments were initiated when mice were 12 weeks old. The HCD (TD.90221, Harlan Teklad) contains 37% fat calories, 1.5% cholesterol, and 0.5% sodium cholate. Both male and female *Sort1* KO mice showed protection against HCD-induced liver injury. Further mechanistic studies were conducted only in female mice, and the results are presented in this study. All animal protocols were approved by the Institutional Animal Care and Use Committee.

Recombinant Adenovirus—Ad-scramble and Ad-null were purchased from Vector Biolabs (Philadelphia, PA). Ad-shCES1 was a generous gift from Dr. Yanqiao Zhang (Northeast Ohio Medical University, Rootstown, OH) (22). Ad-hSORT1-FLAG was generated as described previously (36). Mice were injected at a dose of 1×10^9 pfu/mouse via tail vein.

Identification of SORT1-interacting Proteins—HepG2 cells were infected with Ad-null (negative control) or Ad-hSORT1-FLAG. C57BL/6J mice were injected with 1×10^9 pfu/mouse Ad-null or Ad-hSORT1-FLAG via tail vein (three mice/group). Livers were collected 5 days after injection. HepG2 cell lysates or pooled liver lysates were used for co-immunoprecipitation with anti-FLAG (M2) antibody conjugated to magnetic beads (Sigma). Precipitated proteins were resolved by SDS-PAGE and used for protein identification by LC-MS/MS (performed by MS Bioworks, Ann Arbor, MI).

Measurement of Biliary Secretion and Bile Acid Composition—Biliary secretion was measured following a previously published method (42). Briefly, WT and *Sort1* KO mice were fed an HCD for 1 week and fasted overnight. After anesthesia, an ~2-cm incision was made to expose the liver and the gallbladder. The gallbladder was then cannulated with PE-10 tubing and secured with double ligation. Bile was collected by gravity into an Eppendorf tube. The bile collected for the first 10 min was discarded. Bile collected for an additional 60 min was used for bile acid, cholesterol, and phospholipid measurements with assay kits. Gallbladder bile acid composition was determined by mass spectrometry as described previously (43).

Metabolomics Analysis of Hepatic Lipids and Bile Acids—Metabolomics analysis of hepatic lipids and bile acids was performed by Metabolon Inc. (Durham, NC). Briefly, recovery standards were added based on tissue weight prior to sample extraction for data normalization. The resulting liver extract was analyzed on a Waters ACQUITY Ultra Performance Liquid Chromatography and a Thermo Scientific Q-Exactive high resolution/accurate mass spectrometer interfaced with a heated electrospray ionization (HESI-II) source and Orbitrap mass analyzer operated at 35,000 mass resolution. Raw data were extracted and then peak-identified using Metabolon's reference library and software. No standard curve was used, and results were expressed as relative peak area under the curve.

Lipid Analysis—Cholesterol and triglyceride were measured with colorimetric assay kits as described previously (9). Pooled plasma from 5–7 mice was used for FPLC analysis of the lipoprotein profile, which was conducted by the Mouse Metabolic Phenotyping Center (MMPC) at the University of Cincinnati.

Western Blotting—Cell lysates or liver homogenates were incubated in radioimmunoprecipitation assay buffer containing 1% SDS and protease inhibitors for 1 h on ice and sonicated briefly. Supernatant after centrifugation was used for SDS-PAGE and immunoblotting. The ImageJ software was used to quantify band intensity.

Real-time PCR—SYBR primers (Bio-Rad, Hercules, CA) were used in real-time PCR. Amplification of 18S was used for normalization. Relative mRNA expression was calculated using the comparative CT (Ct) method and expressed as $2^{-\Delta\Delta Ct}$.

Immunofluorescence Imaging—HepG2 cells were fixed in 4% paraformaldehyde and permeabilized in 0.1% Tween 20 and 0.3 M glycine. Primary antibodies and Alexa Fluor-conjugated secondary antibodies were used for immunofluorescent staining. Images were acquired with either a Leica DM 5500 confocal microscope at the Kansas University Medical Center (KUMC) or a STED type super-resolution microscope (Leica TSC SP8 STED 3X) at the Molecular Cytology Core at the University of Missouri.

Statistical Analysis—Results were expressed as mean ± S.E. unless noted. Statistical analysis was performed by Student's *t* test. A $p < 0.05$ was considered statistically significant.

Author Contributions—J. L., Y. W., and D. J. M. were involved in experimental design and conducted experiments and data collection. H. C. and P. K. determined the mitochondrial function. F. L. performed bile acid analysis. T. L. supervised the study and wrote the manuscript.

Acknowledgments—We gratefully thank Dr. Yanqiao Zhang (Northeast Ohio Medical University, Rootstown, OH) for providing the AdshCES1. We gratefully thank Dr. Richard Lehner (University of Alberta, Edmonton, Alberta, Canada) for providing the frozen liver tissue of Ces1 (Es-X) and Ces3 (Tgh) knock-out mice for antibody validation. We thank Robert Davison (Leica Microsystems) for assistance in acquiring STED microscope images.

References

1. Hermey, G. (2009) The Vps10p-domain receptor family. *Cell. Mol. Life Sci.* **66,** 2677–2689
2. Canuel, M., Korkidakis, A., Konnyu, K., and Morales, C. R. (2008) Sortilin mediates the lysosomal targeting of cathepsins D and H. *Biochem. Biophys. Res. Commun.* **373,** 292–297
3. Musunuru, K., Strong, A., Frank-Kamenetsky, M., Lee, N. E., Ahfeldt, T., Sachs, K. V., Li, X., Li, H., Kuperwasser, N., Ruda, V. M., Pirruccello, J. P., Muchmore, B., Prokunina-Olsson, L., Hall, J. L., Schadt, E. E., *et al.* (2010) From noncoding variant to phenotype via *SORT1* at the 1p13 cholesterol locus. *Nature* **466,** 714–719
4. Kathiresan, S., Melander, O., Guiducci, C., Surti, A., Burtt, N. P., Rieder, M. J., Cooper, G. M., Roos, C., Voight, B. F., Havulinna, A. S., Wahlstrand, B., Hedner, T., Corella, D., Tai, E. S., Ordovas, J. M., *et al.* (2008) Six new loci associated with blood low-density lipoprotein cholesterol, high-density lipoprotein cholesterol or triglycerides in humans. *Nat. Genet.* **40,** 189–197
5. Myocardial Infarction Genetics Consortium, Kathiresan, S., Voight, B. F., Purcell, S., Musunuru, K., Ardissino, D., Mannucci, P. M., Anand, S., Engert, J. C., Samani, N. J., Schunkert, H., Erdmann, J., Reilly, M. P., Rader, D. J., Morgan, T., Spertus, J. A., *et al.* (2009) Genome-wide association of early-onset myocardial infarction with single nucleotide polymorphisms and copy number variants. *Nat. Genet.* **41,** 334–341
6. Kjolby, M., Andersen, O. M., Breiderhoff, T., Fjorback, A. W., Pedersen, K. M., Madsen, P., Jansen, P., Heeren, J., Willnow, T. E., and Nykjaer, A. (2010) *Sort1*, encoded by the cardiovascular risk locus 1p13.3, is a regulator of hepatic lipoprotein export. *Cell Metab.* **12,** 213–223
7. Gustafsen, C., Kjolby, M., Nyegaard, M., Mattheisen, M., Lundhede, J., Buttenschøn, H., Mors, O., Bentzon, J. F., Madsen, P., Nykjaer, A., and Glerup, S. (2014) The hypercholesterolemia-risk gene *SORT1* facilitates PCSK9 secretion. *Cell Metab.* **19,** 310–318
8. Butkinaree, C., Canuel, M., Essalmani, R., Poirier, S., Benjannet, S., Asselin, M. C., Roubtsova, A., Hamelin, J., Marcinkiewicz, J., Chamberland, A., Guillemot, J., Mayer, G., Sisodia, S. S., Jacob, Y., Prat, A., and Seidah, N. G. (2015) Amyloid precursor-like protein 2 and sortilin do not regulate the PCSK9 convertase-mediated low density lipoprotein receptor degradation but interact with each other. *J. Biol. Chem.* **290,** 18609–18620
9. Li, J., Bi, L., Hulke, M., and Li, T. (2014) Fish oil and fenofibrate prevented phosphorylation-dependent hepatic sortilin 1 degradation in Western diet-fed mice. *J. Biol. Chem.* **289,** 22437–22449
10. Bi, L., Chiang, J. Y., Ding, W. X., Dunn, W., Roberts, B., and Li, T. (2013) Saturated fatty acids activate ERK signaling to downregulate hepatic sortilin 1 in obese and diabetic mice. *J. Lipid Res.* **54,** 2754–2762
11. Puri, P., Baillie, R. A., Wiest, M. M., Mirshahi, F., Choudhury, J., Cheung, O., Sargeant, C., Contos, M. J., and Sanyal, A. J. (2007) A lipidomic analysis of nonalcoholic fatty liver disease. *Hepatology* **46,** 1081–1090
12. Caballero, F., Fernández, A., De Lacy, A. M., Fernández-Checa, J. C., Caballería, J., and García-Ruiz, C. (2009) Enhanced free cholesterol, SREBP-2 and StAR expression in human NASH. *J. Hepatol.* **50,** 789–796
13. Marí, M., Caballero, F., Colell, A., Morales, A., Caballeria, J., Fernandez, A., Enrich, C., Fernandez-Checa, J. C., and García-Ruiz, C. (2006) Mitochondrial free cholesterol loading sensitizes to TNF- and Fas-mediated steatohepatitis. *Cell Metab.* **4,** 185–198
14. Matsuzawa, N., Takamura, T., Kurita, S., Misu, H., Ota, T., Ando, H., Yokoyama, M., Honda, M., Zen, Y., Nakanuma, Y., Miyamoto, K., and Kaneko, S. (2007) Lipid-induced oxidative stress causes steatohepatitis in mice fed an atherogenic diet. *Hepatology* **46,** 1392–1403
15. Wouters, K., van Gorp, P. J., Bieghs, V., Gijbels, M. J., Duimel, H., Lütjohann, D., Kerksiek, A., van Kruchten, R., Maeda, N., Staels, B., van Bilsen, M., Shiri-Sverdlov, R., and Hofker, M. H. (2008) Dietary cholesterol, rather than liver steatosis, leads to hepatic inflammation in hyperlipidemic mouse models of nonalcoholic steatohepatitis. *Hepatology* **48,** 474–486
16. Van Rooyen, D. M., Larter, C. Z., Haigh, W. G., Yeh, M. M., Ioannou, G., Kuver, R., Lee, S. P., Teoh, N. C., and Farrell, G. C. (2011) Hepatic free cholesterol accumulates in obese, diabetic mice and causes nonalcoholic steatohepatitis. *Gastroenterology* **141,** 1393–1403, 1403.e1–5
17. Hendrikx, T., Walenbergh, S. M., Hofker, M. H., and Shiri-Sverdlov, R. (2014) Lysosomal cholesterol accumulation: driver on the road to inflammation during atherosclerosis and non-alcoholic steatohepatitis. *Obes. Rev.* **15,** 424–433
18. Gan, L. T., Van Rooyen, D. M., Koina, M. E., McCuskey, R. S., Teoh, N. C., and Farrell, G. C. (2014) Hepatocyte free cholesterol lipotoxicity results from JNK1-mediated mitochondrial injury and is HMGB1 and TLR4-dependent. *J. Hepatol.* **61,** 1376–1384
19. Wang, Y., Ding, Y., Li, J., Chavan, H., Matye, D., Ni, H.-M., Chiang, J. Y. L., Krishnamurthy, P., Ding, W.-X., and Li, T. (2016) Targeting the enterohepatic bile acid signaling induces hepatic autophagy via a CYP7A1-AKT-mTOR axis in mice. *Cell. Mol. Gastroenterol. Hepatol.* 10.1016/j.jcmgh.2016.10.002
20. Zhao, B., Natarajan, R., and Ghosh, S. (2005) Human liver cholesteryl ester hydrolase: cloning, molecular characterization, and role in cellular cholesterol homeostasis. *Physiol. Genomics* **23,** 304–310
21. Ko, K. W., Erickson, B., and Lehner, R. (2009) Es-x/Ces1 prevents triacylglycerol accumulation in McArdle-RH7777 hepatocytes. *Biochim. Biophys. Acta* **1791,** 1133–1143
22. Xu, J., Li, Y., Chen, W. D., Xu, Y., Yin, L., Ge, X., Jadhav, K., Adorini, L., and Zhang, Y. (2014) Hepatic carboxylesterase 1 is essential for both normal and farnesoid X receptor-controlled lipid homeostasis. *Hepatology* **59,** 1761–1771
23. Bie, J., Wang, J., Yuan, Q., Kakiyama, G., Ghosh, S. S., and Ghosh, S. (2014) Liver-specific transgenic expression of cholesteryl ester hydrolase reduces atherosclerosis in $Ldlr^{-/-}$ mice. *J. Lipid Res.* **55,** 729–738
24. Quiroga, A. D., Li, L., Trötzmüller, M., Nelson, R., Proctor, S. D., Köfeler, H., and Lehner, R. (2012) Deficiency of carboxylesterase 1/esterase-x results in obesity, hepatic steatosis, and hyperlipidemia. *Hepatology* **56,** 2188–2198
25. Zhao, B., Song, J., Chow, W. N., St Clair, R. W., Rudel, L. L., and Ghosh, S. (2007) Macrophage-specific transgenic expression of cholesteryl ester hydrolase significantly reduces atherosclerosis and lesion necrosis in $Ldlr^{-/-}$ mice. *J. Clin. Invest.* **117,** 2983–2992
26. Zhao, B., Song, J., and Ghosh, S. (2008) Hepatic overexpression of cholesteryl ester hydrolase enhances cholesterol elimination and *in vivo* reverse cholesterol transport. *J. Lipid Res.* **49,** 2212–2217
27. Beltroy, E. P., Richardson, J. A., Horton, J. D., Turley, S. D., and Dietschy, J. M. (2005) Cholesterol accumulation and liver cell death in mice with Niemann-Pick type C disease. *Hepatology* **42,** 886–893
28. Chavez, J. A., and Summers, S. A. (2012) A ceramide-centric view of insulin resistance. *Cell Metab.* **15,** 585–594
29. Wang, S., Robinet, P., Smith, J. D., and Gulshan, K. (2015) ORMDL orosomucoid-like proteins are degraded by free-cholesterol-loading-induced autophagy. *Proc. Natl. Acad. Sci. U.S.A.* **112,** 3728–3733
30. Raichur, S., Wang, S. T., Chan, P. W., Li, Y., Ching, J., Chaurasia, B., Dogra, S., Öhman, M. K., Takeda, K., Sugii, S., Pewzner-Jung, Y., Futerman, A. H., and Summers, S. A. (2014) CerS2 haploinsufficiency inhibits β-oxidation

and confers susceptibility to diet-induced steatohepatitis and insulin resistance. *Cell Metab.* **20,** 687–695
31. García-Ruiz, C., Colell, A., Marí, M., Morales, A., Calvo, M., Enrich, C., and Fernández-Checa, J. C. (2003) Defective TNF-α-mediated hepatocellular apoptosis and liver damage in acidic sphingomyelinase knockout mice. *J. Clin. Invest.* **111,** 197–208
32. Ni, X., and Morales, C. R. (2006) The lysosomal trafficking of acid sphingomyelinase is mediated by sortilin and mannose 6-phosphate receptor. *Traffic* **7,** 889–902
33. Rabinowich, L., Fishman, S., Hubel, E., Thurm, T., Park, W. J., Pewzner-Jung, Y., Saroha, A., Erez, N., Halpern, Z., Futerman, A. H., and Zvibel, I. (2015) Sortilin deficiency improves the metabolic phenotype and reduces hepatic steatosis of mice subjected to diet-induced obesity. *J. Hepatol.* **62,** 175–181
34. Li, T., and Chiang, J. Y. (2014) Bile acid signaling in metabolic disease and drug therapy. *Pharmacol. Rev.* **66,** 948–983
35. Bahitham, W., Watts, R., Nelson, R., Lian, J., and Lehner, R. (2016) Liver-specific expression of carboxylesterase 1g/esterase-x reduces hepatic steatosis, counteracts dyslipidemia and improves insulin signaling. *Biochim. Biophys. Acta* **1861,** 482–490
36. Li, J., Matye, D. J., and Li, T. (2015) Insulin resistance induces post-translational hepatic sortilin 1 degradation in mice. *J. Biol. Chem.* **290,** 11526–11536
37. Canuel, M., Lefrancois, S., Zeng, J., and Morales, C. R. (2008) AP-1 and retromer play opposite roles in the trafficking of sortilin between the Golgi apparatus and the lysosomes. *Biochem. Biophys. Res. Commun.* **366,** 724–730
38. Yuan, Q., Bie, J., Wang, J., Ghosh, S. S., and Ghosh, S. (2013) Cooperation between hepatic cholesteryl ester hydrolase and scavenger receptor BI for hydrolysis of HDL-CE. *J. Lipid Res.* **54,** 3078–3084
39. Henkel, A. S., Anderson, K. A., Dewey, A. M., Kavesh, M. H., and Green, R. M. (2011) A chronic high-cholesterol diet paradoxically suppresses hepatic CYP7A1 expression in FVB/NJ mice. *J. Lipid Res.* **52,** 289–298
40. Li, T., Jahan, A., and Chiang, J. Y. (2006) Bile acids and cytokines inhibit the human cholesterol 7α-hydroxylase gene via the JNK/c-jun pathway in human liver cells. *Hepatology* **43,** 1202–1210
41. Ikonen, E. (2006) Mechanisms for cellular cholesterol transport: defects and human disease. *Physiol. Rev.* **86,** 1237–1261
42. Baghdasaryan, A., Fuchs, C. D., Österreicher, C. H., Lemberger, U. J., Halilbasic, E., Påhlman, I., Graffner, H., Krones, E., Fickert, P., Wahlström, A., Ståhlman, M., Paumgartner, G., Marschall, H. U., and Trauner, M. (2016) Inhibition of intestinal bile acid absorption improves cholestatic liver and bile duct injury in a mouse model of sclerosing cholangitis. *J. Hepatol.* **64,** 674–681
43. Li, T., Francl, J. M., Boehme, S., Ochoa, A., Zhang, Y., Klaassen, C. D., Erickson, S. K., and Chiang, J. Y. (2012) Glucose and insulin induction of bile acid synthesis: mechanisms and implication in diabetes and obesity. *J Biol. Chem.* **287,** 1861–1873